SCIENCE CHINA
Technological Sciences

• Article •

November 2014 Vol.57 No.11: 2089–2095
doi: 10.1007/s11431-014-5657-3

Compatible hybrid 3D printing of metal and nonmetal inks for direct manufacture of end functional devices

WANG Lei[1] & LIU Jing[1,2*]

[1] *Beijing Key Laboratory of CryoBiomedical Engineering and Key Laboratory of Cryogenics, Technical Institute of Physics and Chemistry, Chinese Academy of Sciences, Beijing 100190, China;*
[2] *Department of Biomedical Engineering, School of Medicine, Tsinghua University, Beijing 100084, China*

Received June 9, 2014; accepted August 1, 2014; published online September 29, 2014

The currently available 3D printing still cannot simultaneously deal with the metal and nonmetal inks together due to their huge difference in the melting points and poor compatible printability between each other. Here through introducing the low melting point alloy $Bi_{35}In_{48.6}Sn_{16}Zn_{0.4}$ and silicone rubber as functional inks, we proposed a compatible hybrid 3D printing method for manufacturing the desired device, the supporting substrate and the allied package structure together. The principle of pneumatic-typed 3D printing of multiple inks was described and typical physical properties of the ink $Bi_{35}In_{48.6}Sn_{16}Zn_{0.4}$ were measured. Several key factors dominating the printing quality such as the temperature of the printing head, the air pressure exerted upon the liquid metal ink in the syringe, the moving velocity and the height of the printing head etc. were clarified. A general way of directly printing out 3D structured electronic devices consisting of both metal and nonmetal materials was demonstrated. Such hybrid objects were patterned and formed up layer by layer with $Bi_{35}In_{48.6}Sn_{16}Zn_{0.4}$ alloy and silicone rubber which would become solidified after standing for a period of time under room temperature. To illustrate the compatible printability of these printing inks, a three-layer tricolor LED stereo circuit with controlled lighting capability was further manufactured and evaluated. The present study opens an important hybrid 3D printing way for directly manufacturing functional and structural end devices in an easy and low cost way.

liquid metal ink, hybrid 3D printing, compatible manufacture, electronic device, stereo circuit

Citation: Wang L, Liu J. Compatible hybrid 3D printing of metal and nonmetal inks for direct manufacture of end functional devices . Sci China Tech Sci, 2014, 57: 2089–2095, doi: 10.1007/s11431-014-5657-3

1 Introduction

Rapid prototyping or 3D printing, as a quickly developing technology, holds strong promise in a wide variety of application areas including chemical synthesis [1], tissue engineering [2,3], microfluidics [4], electronic circuit and device [5], etc. To date, laser sintering (LS), laser melting (LM) and laser metal deposition (LMD) are among three most prevailing techniques that are capable of printing 3D objects with high melting point metals, alloys and metal matrix composites (MMCs) [6]. The printing quality is generally affected by such factors like the chemical constituents of the powder materials, powder flowability, laser administration process [6–8] etc. For this reason, the currently available printable metal inks at room temperature are rather limited. Compared to the laser-based printing method, pneumatic-typed liquid metal 3D printing as will be tackled in this paper owns several advantages such as low cost, easy deposition on different substrates, and straightforward to realize hybrid 3D printing which is a most important virtue for making end products.

*Corresponding author (email: jliu@mail.ipc.ac.cn)

Clearly, identification of candidate inks with suitable melting point is the key to determine whether pneumatic-typed liquid metal 3D printing will work smoothly or not. In recent years, low melting point metal has attracted more and more attention as electronic ink in the direct writing of electronics and 3D printing. The present lab had ever developed a desktop printing method of flexible circuits on paper with liquid metal ink [9]. Additional work was also performed to investigate the way to write liquid metal microcomponents at room temperature [10]. In some studies, the soft-lithography fabrication has been applied to pattern the liquid-phase electronic circuits on an elastomer substrate with gallium-indium alloy [11]. With the continuous efforts, the relationships between nozzle inner diameter, standoff distance, flow rate, and the resulting trace geometry gradually become clear [12]. In these studies, $GaIn_{24.5}$ alloy was mainly adopted as the printing material whose outstanding merit lies in its rather easy printability due to the low melting point (~15.7°C). An only pity is that, with such metal ink, the fabricated 3D metal objects may subject to melt at around room temperature. Therefore, more favorable metal ink materials, which are printable at room temperature and could easily solidify at a slightly higher temperature above ambient condition, need to be investigated. In this regard, the melting point of the metal ink should be larger than room temperature, which however will not be too high for practically operational purpose (such as below 300°C).

From the academic aspect, hybrid 3D printing is an important direction in the printing technology field, which combines different printing techniques or ink materials to achieve better properties of the printed objects such as the fabrication of 3D polymeric scaffolds [13]. It has been demonstrated that dual-color polymer light-emitting pixels could be made by using hybrid inkjet printing technology, which combined a pin-hole free polymer buffer layer and an inkjet-printed polymer layer [14]. Multi-nozzle drop-on demand printing system was also adopted to dispense a wide range of functional materials using various types of dispensing nozzles [15]. A hybrid inkjet printing/electrospinning system had even been used to fabricate viable tissues for cartilage tissue engineering applications [16]. Through 3D printing of a cell-seeded hydrogel matrix in the anatomic geometry of a human ear, along with an intertwined conducting polymer consisting of infused silver nanoparticles, a bionic ear was also made possible [17]. However, all these printings are based mainly on nonmetal materials. Until now, hybrid printing of metal and nonmetal inks together to compose functional devices still remained a big challenge due to the huge difference between the melting points of existing metal inks and that of nonmetal materials.

In this study, we present for the first time a fundamental way to directly print out 3D structures and electronic devices consisting of low melting point liquid metal and nonmetal materials. The working mechanisms lying behind will be interpreted. As a proof of this hybrid 3D printing concept, a three-layer tricolor LED stereo circuit incorporated with functional and structural properties will be demonstrated.

2 Materials and methods

2.1 Preparation of printable metal inks

Four kinds of metals (bismuth, indium, tin and zinc) with the purity above 99.99% (4 N) were weighed according to the ratio of 35:48.6:16:0.4. These pure metals were put in a beaker for 5 hours at 245°C in an electric vacuum drying oven. Then, the mixture was stirred in the beaker which was put in water bath at 85–90°C for 30 min. Finally, the beaker was kept in the electric vacuum drying oven at 245°C for 2 hours to further ensure a well-mixed alloy solution.

2.2 Experimental devices

The electrical conductivity-temperature curve and thermal conductivity-temperature curve of $Bi_{35}In_{48.6}Sn_{16}Zn_{0.4}$ were measured by four-probe electrometer method using a physical property measurement system (PPMS, Quantum Design) with a heating rate of 5°C/min in the temperature range from −140 to 36°C, respectively. The thermal expansion rate-temperature curve and thermal expansion coefficient-temperature curve of $Bi_{35}In_{48.6}Sn_{16}Zn_{0.4}$ were measured through a dilatometer (L75, LINSEIS, Germany) with a heating rate of 5°C/min in the temperature range from –140 to 49°C. The contact angle of the $Bi_{35}In_{48.6}Sn_{16}Zn_{0.4}$ droplet on the solid-state 705 silicone rubber substrate as shown in Figure 3(b) was measured through a contact angle meter (JC2000D3, Shanghai). The values of the printed capacitor and inductor as shown in Figure 3(f) and (g) were measured through a digital electric bridge. The melting point of $Bi_{35}In_{48.6}Sn_{16}Zn_{0.4}$ was measured through a differential scanning calorimeter instrument (DSC200, NETZSCH, Germany) with ramping rate of 10°C/min under N_2 atmosphere.

3 Results and discussion

3.1 The principle of the pneumatic-typed 3D printing

In order to ensure that the metal ink is always in liquid-state before printing, the printing head needs to be heated during running of the machine. The structure of the printing head used in the present study shown in Figure 1(a) is designed as follows: A syringe cylinder is wrapped in a heating copper block with the conductive constantan wire winding around it. The electrical current through the constantan wire is regulated to hold the liquid metal ink in the syringe cylinder at a temperature higher than the melting point of

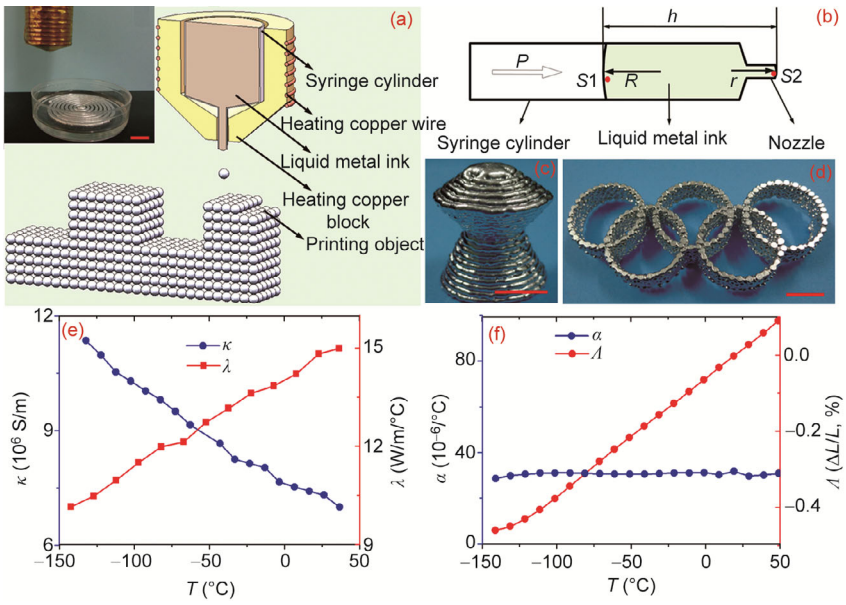

Figure 1 The printing schematic and the property curves of the metal ink $Bi_{35}In_{48.6}Sn_{16}Zn_{0.4}$. (a) The schematic view of the liquid metal 3D printing and the printing head structure. Inset: The photo of the printing head; (b) graphic illustration of pneumatic-typed liquid metal printing; (c) and (d) the printing articles through using the pneumatic-typed liquid metal printing method; (e) κ (the electrical conductivity)-T (temperature) and λ (the thermal conductivity)-T (temperature) measurement curves of the liquid metal ink $Bi_{35}In_{48.6}Sn_{16}Zn_{0.4}$; (f) α (the thermal expansion coefficient)-T (temperature) and Λ (the thermal expansion rate)-T (temperature) measurement curves of the liquid metal ink $Bi_{35}In_{48.6}Sn_{16}Zn_{0.4}$. Scale bars in (a), (c) and (d) are all 10 mm in length.

the ink. The exterior photo of the printing head is presented in the inset of Figure 1(a), and the principle of the pneumatic-typed liquid metal 3D printing method adopted here is shown in Figure 1(b). Assuming that the curvature radiuses of the top and the bottom convex surfaces of the liquid metal in the syringe cylinder are R and r, respectively. The surface tension coefficient and the density of the liquid metal ink, acceleration of the gravity and the atmospheric pressure are represented as σ, ρ, g and P_0, respectively. $S1$ and $S2$ are two points in the liquid metal ink near the centers of the top and the bottom convex surfaces respectively and the distance between them is represented as h. According to the basic equation of fluid statics, the pressure relationship between $S1$ and $S2$ can be expressed as

$$P_{S2} = P_{S1} + \rho g h. \tag{1}$$

Besides, the pressure below the surface is equal to the pressure above the surface plus additional pressure. And the pressures at $S1$ and $S2$ can be respectively written as

$$P_{S1} = P_0 + 2\sigma / R, \tag{2}$$

$$P_{S2} = P_0 + 2\sigma / r. \tag{3}$$

Through substituting eqs. (2) and (3) into eq. (1) for each species, one has

$$P_0 + 2\sigma / R + \rho g h = P_0 + 2\sigma / r. \tag{4}$$

Obviously, R should be larger than r on condition that $h > 0$. When the pressure above the top surface of liquid metal is increased from P_0 to P_0+P, r should be decreased to maintain the system pressure balance. With the increase of P, r becomes smaller and smaller and a liquid metal droplet is gradually formed below the printing head. Eventually the droplet falls from the printing head due to gravity effect and a second one will follow and repeat the same procedure.

3.2 Typical printing properties of the liquid metal ink

To perform the pneumatic-typed liquid metal 3D printing method, $Bi_{35}In_{48.6}Sn_{16}Zn_{0.4}$ was introduced as the metal ink whose density (7.898 g/cm^3) is close to that of iron (7.86 g/cm^3). Such alloy is not easy to be oxidized and a detailed preparation procedure for this material is mentioned above. Until now, few trials were made on such material for 3D printing. Figures 1(c) and (d) present the printing articles with metallic luster indicating that this metal ink is subjected to negligible oxidation during printing process. With melting point and subcooling degree repectively as 58.3 and 2.4°C, such alloy could complete its solid-liquid phase transition over a temperature range of 50–60°C. The melting enthalpy and specific heat capacity of $Bi_{35}In_{48.6}Sn_{16}Zn_{0.4}$ are respectively measured as 28.94 J/g and 0.262 J/(g °C), which are much smaller compared to that of common metals such as aluminum (393.0 J/g and 0.88 J/(g °C), respectively). These properties enable the molten droplets of $Bi_{35}In_{48.6}Sn_{16}Zn_{0.4}$ to be cooled in a very short time at room temperature.

Through measurement, the κ (the electrical conductivity)-T (temperature) and λ (the thermal conductivity)-T (tem-

perature) curves for $Bi_{35}In_{48.6}Sn_{16}Zn_{0.4}$ are depicted in Figure 1(e). It can be observed that with the increase of T over the temperature range of −140–36°C, λ approximates to a linear increase while κ approximates to a linear decrease. Such opposite changing trends can be interpreted as follows: The heat conduction of the solid-state alloy depends mainly upon the lattice vibration [18] induced by atomic motions. As the temperature of the alloy increases, the irregular motion of the alloy atoms and the lattice vibration are intensified. This increases the thermal conductivity of the alloy which is a measure of how fast heat will be conducted. On the other hand, the vibrating lattices hinder the motion of free electrons and the electrical conductivity of the alloy which measures a material's ability to conduct an electric current will thus decrease. The electrical and thermal conductivity properties of $Bi_{35}In_{48.6}Sn_{16}Zn_{0.4}$ enable it to be used as the metal ink for printing conductive objects and heat conductor. The α (the thermal expansion coefficient)-T (temperature) and Λ (the thermal expansion rate)-T (temperature) measurement curves of $Bi_{35}In_{48.6}Sn_{16}Zn_{0.4}$ are shown in Figure 1(f). It can be seen that there is a strong linear relationship between Λ and T, while α-T curve is nearly a horizontal line in the temperature range of −140–49°C. Here α and Λ are respectively defined as

$$\alpha=\frac{\Delta L}{L}=\frac{L_T-L_{20}}{L_{20}}, \tag{5}$$

$$\Lambda=\frac{\alpha}{\Delta T}=\frac{\alpha}{T-20}, \tag{6}$$

where L_T and L_{20} are the sample length at temperature T and 20°C, respectively. Although $Bi_{35}In_{48.6}Sn_{16}Zn_{0.4}$ has the property of cold shrinkage and thermal expansion, its thermal expansion coefficient (from about 28×10^{-6}/°C to about 32×10^{-6}/°C in the range of temperature –140–49°C) is so small that the printed line has only small deformation when it is cooled to solid.

3.3 Parameter features of the printing system

In this section, the printing system parameter settings using the pneumatic-typed liquid metal 3D printing method are investigated. The inner diameter of the printing head is 60 μm in all the experiments. The critical system parameters include the temperature of the printing head (T), the air pressure exerted upon the liquid metal ink in the syringe (P), the moving velocity (V) of the printing head, and the distance between the printing head and the substrate (H). The latter three are represented in Figure 2(a), as well as the diameter (M) of the droplet fall on the substrate and the distance (D) between two adjacent droplets. In order to ensure the continuous delivery of the liquid metal drops from the printing head, the metal ink contained in the syringe cylinder should be heated to between about 80 and 90°C. Figure 2(b) shows the changing trends of M and D with the increase of P when the printing head is at different height. As the pressure is increased to a certain value, M equals to D which means that adjacent droplets fell on the substrate being serially connected. This pressure is almost a fixed value at different heights and it can be called as critical pressure P_c. Different V corresponds to different P_c, and the curve relationship between them is shown as the real line in Figure 2(c). On the one hand, P should be equal to or greater than P_c to ensure the printing of continous lines. But on the other hand, P should be lower than $1.1P_c$ in the printing process. Otherwise the overlapping part of adjacent droplets on the substrate will be too much and the printing resolution will thus be reduced. Therefore P values (when V within the range of 0–5 mm/s) are selected in the area between the solid and dashed lines in Figure 2(c). Figure 2(d) shows the M-H and D-H relationships on condition that the velocity of the printing head is set as 3 mm/s. When H is decreased from 20 mm to about 1 mm, a slow descending tendency of M and a slow ascending tendency of D are observed. But M and D decrease drastically as H becomes larger than 1 mm and H=1 mm can be deemed as a demarcation line. This is mainly because that a droplet has contacted the substrate before its departure of the printing head when H<1 mm, and subsequently the droplet will remain on the substrate due to the frictional resistance of the substrate surface. With the decrease of H, the distance between two adjacent droplets becomes more and more larger, which has a bad effect on the printing quality.

3.4 Strategies of hybrid 3D printing

In this study, a combined printing between metal and nonmetal materials with very different physical properties are introduced which is the first trial in the area. The alloy $Bi_{35}In_{48.6}Sn_{16}Zn_{0.4}$ as mentioned above and 705 silicone rubber are selected as metal and nonmetal inks respectively. As is known, 705 silicone rubber is a kind of neutral transparent single component RTV (room temperature vulcanizing) silicone rubber, which would be solidified after absorbing the water in air at room temperature. It is non-toxic, free from corrosion, electrically insulated, anti-electric arc and can be used between –60–150°C with excellent bonding property. Previously, this material is mainly applied for encapsulating and sealing the electrical components to resist dampness and shock, thus stabilizing the property of the components. Several mechanical parameters of the solidified 705 silicone rubber are as follows: The tensile strength, shear strength, tensile elongation and hardness Shore A read as 0.4, 0.5 MPa, 100% and 15, respectively. The 705 silicone rubber is self-leveling and does not need heating when it is administrated as the ink during printing. After curing for 3–30 min, its curing depth is 2–3 mm at room temperature and 50% relative humidity environment after

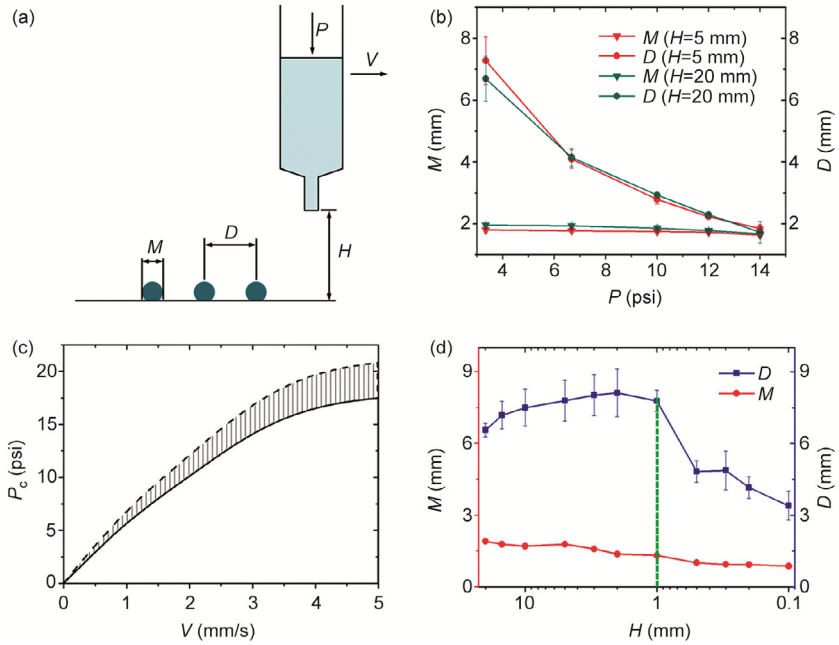

Figure 2 (a) Representation of parameters *P*, *V*, *M*, *D* and *H*; (b) the *M* (diameter)-*P* (pressure) and *D* (distance)-*P* (pressure) relationships when *H*=5 mm and *H*=20 mm, respectively. Errorbars represent the standard deviation of the mean; (c) the curve relationship between P_c (critical pressure) and *V* (velocity) over the range of 0–5 mm/s; (d) the *M* (diameter)-*P* (pressure) and *D* (distance)-*P* (pressure) relationships when *V*=3 mm/s. Errorbars represent the standard deviation of the mean.

24 hours. Its good strength and flexibility enable the sealed components not to easily suffer from damaging. The pressure in the syringe is maintained in the range from about 0.05 to 0.1 MPa and the inner diameter of the printing head is 0.84 mm when 705 silicone rubber is used as the printing ink. The fabrication process of the hybrid objects as shown in Figure 3(a) begins by printing a layer of several-millimeter-thick silicone rubber on the bottom of an empty plastic petri dish with a 705 silicone rubber nozzle. This transparent colloid will flatten out due to its self-leveling property and become fully solidified at normal humidity after 24 hours later. Then the metal structures are printed on the surface of the first layer with the $Bi_{35}In_{48.6}Sn_{16}Zn_{0.4}$ ink and the printed structures will be solidified in several seconds. After this step, a second layer of 705 silicone rubber is printed above the metal layer and the solidification time is similar to that of step one. Finally the printed hybrid object with three-layer hamburger structure is taken out of the plastic petri dish. Figure 3(b) shows a $Bi_{35}In_{48.6}Sn_{16}Zn_{0.4}$ droplet on the solid-state 705 silicone rubber substrate and its contact angle value is measured as 108°±1°, while Figure 3(c) shows several $Bi_{35}In_{48.6}Sn_{16}Zn_{0.4}$ droplets in the liquid-state 705 silicone rubber which indicates the good compatibility between the metal droplets and

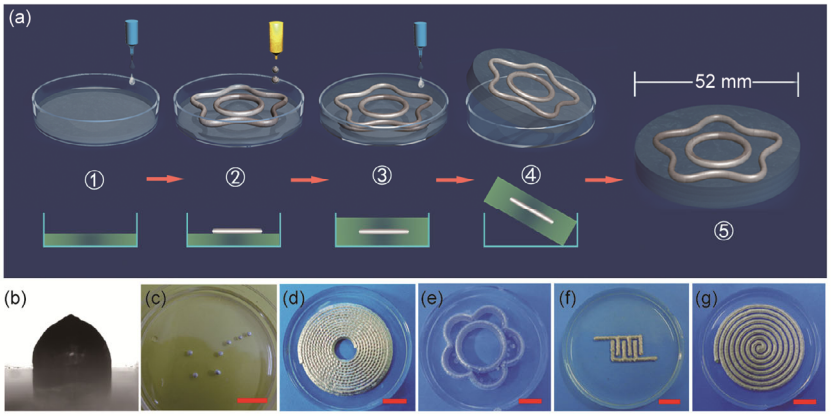

Figure 3 The process of hybrid 3D printing and several typical production examples. (a) Hybrid 3D printing process with $Bi_{35}In_{48.6}Sn_{16}Zn_{0.4}$ and 705 silicone rubber inks; (b) the $Bi_{35}In_{48.6}Sn_{16}Zn_{0.4}$ droplet on the solid-state 705 silicone rubber substrate; (c) the $Bi_{35}In_{48.6}Sn_{16}Zn_{0.4}$ droplets in the liquid-state 705 silicone rubber; (d) several printed plane structure; (e) the printed stereo structure; (f) the printed comb capacitor; (g) the printed inductor. Scale bars in (c)–(g) are all 10 mm in length.

the silicon rubber. Figures 3(d) and (e) display two printing articles in which the imbedded metal structures are respectively plane and stereo structures. Figures 3(f) and (g) present a printed comb capacitor and a printed inductor with the value of 1.5 pF and 5.9 μH, respectively.

3.5 Printing of three-layer LED stereo circuit

Besides these packaged metal structures and electronic devices, some packaged stereo circuits can also be printed out with the current hybrid 3D printing method. A three-layer LED stereo circuit shown in Figure 4 is printed with $Bi_{35}In_{48.6}Sn_{16}Zn_{0.4}$ and 705 silicone rubber inks. This stereo circuit is composed of six LEDs which are connected to current-limiting resistors respectively. The circuit schematic is shown in Figure 4(a). Both the LEDs and resistors used here are SMD (Surface Mounted Devices) components. The circuit is divided into three layers. The color of the two LEDs in each layer is one of three colors (red, yellow, green) and the value of all the current-limiting resistors is 2 kohm. The whole printed object contains three-layer metal structures and four-layer nonmetal structures, as well as the connecting short columns between adjacent metal layers (the drawing effect of the printed object is presented in Figure 4(b). Before a metal layer is printed, the SMD components are placed according to their positions in the circuit layout with their reverse sides facing upwards. During the printing process, we found that $Bi_{35}In_{48.6}Sn_{16}Zn_{0.4}$ cannot be strongly connected to the copper electrodes of the SMD components. To resolve this problem, a pretreatment to the copper electrode is performed. First, a layer of solder tin (Sn63/Pb37, melting point ~183°C) is attached to the electrode and thereby an intermetallic layer including Cu-Sn alloy is formed between them. Then a layer of printing ink is laid over the solder tin layer and a mixed-metal layer will thus be formed. Here the mixed-metal layer contains the metal elements in both the printing layer and the solder tin layer. This pretreatment improves the connecting reliability between the copper electrode and the printing ink. The structure of the SMD component electrode which has undergone a pretreatment is shown in Figure 4(c). The printed hybrid object is presented in Figure 4(d). When the positive and negative electrodes of the printed circuit are respectively connected to the respective anode and cathode of a 3.7 V Li-ion battery, the LEDs emit bright tricolors (as shown in Figure 4(e)). This LED circuit indicates that functional circuits with spatial three-dimensional structures can be printed out by using low melting point metal and insulated packaging material in an easy way. This is among the very few ever trials in the 3D printing area. The stereo circuit prepared with this low-cost printed method owns several unique characteristics. The mechanical properties such as hardness and shear strength depend mainly on the corresponding properties of the 705 silicone rubber as mentioned above. Besides, this circuit can work normally in

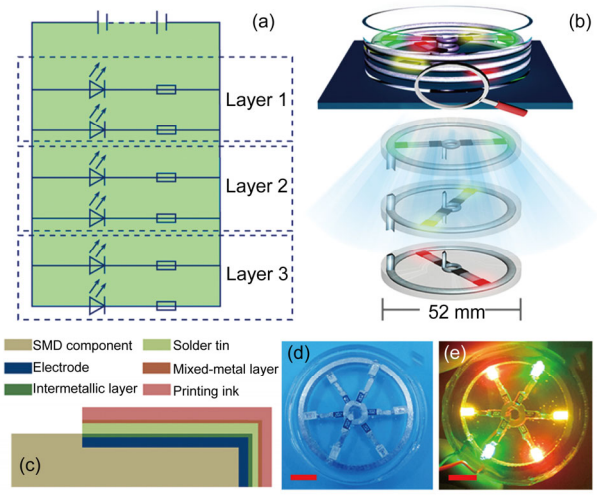

Figure 4 Three-layer LED stereo circuit printed with $Bi_{35}In_{48.6}Sn_{16}Zn_{0.4}$ and 705 silicone rubber. (a) The diagram of the circuit; (b) the schematic drawing of the printed object; (c) the structure of the SMD component electrode to which a pretreatment has been applied; (d) the appearance of the printed object; (e) the photo of the circuit in the electrifying state. Scale bars in (d) and (e) are all 10 mm in length.

any relative humidity envrionment and at the temperature lower than the melting point of liquid metal $Bi_{35}In_{48.6}Sn_{16}Zn_{0.4}$. The circuit printed through the hybrid 3D printing method holds strong practical value. Even though, further investigation should be performed to improve the printing resolution, as well as the connection reliability of the metal ink and the electrodes of the components. The curing time of 705 silicone rubber with several-millimeter-thick is typically about 24 hours at normal humidity, which is too long for the quick printing purpose. To improve the printing efficiency, increasing the humidity of printing environment by utilizing an atomizer or a humidifier can shorten the curing time of 705 silicone rubber to less than 5 hours.

4 Conclusions

In summary, we have established a hybrid 3D metal/nonmetal printing method and demonstrated its practical value for directly manufacturing target functional device. With the introduced liquid metal ink $Bi_{35}In_{48.6}Sn_{16}Zn_{0.4}$ and the packaging material silicone rubber, a highly compatible 3D printing on both metal and nonmetal components are enabled for the first time. The basic mechanism as clarified lies in that the melting point of the compatibly metal ink should be slightly higher than room temperature so as to print out solidified structures in an easy and low-cost way. Further, through a series of conceptual experiments, relationships between the parameters including the temperature and the moving velocity of the printing head, the distance between the printing head and the substrate, as well as the air pressure exerted upon the liquid metal ink in the syringe

are investigated. The hybrid 3D printing method as proposed in this study makes full use of the relatively high mechanical strength and electric conductivity of $Bi_{35}In_{48.6}Sn_{16}Zn_{0.4}$ ink and the excellent insulativity, transparent and good sealing property of 705 silicone rubber ink. Structures and electronic devices including plane and stereo structures, capacitor and inductor were thus printed hybrid with these two kinds of inks. Finally, we demonstrated a three-layer tricolor LED circuit to illustrate the capability of this printing method. It can be forseen that the hybrid 3D printing of low melting point metal and insulated packaging material will help mold an important way for future 3D printing in the coming time.

This work was supported by the Research Funding of the Chinese Academy of Sciences (Grant No. KGZD-EW-T04-4).

1 Symes M D, Kitson P J, Yan J, et al. Integrated 3D-printed reactionware for chemical synthesis and analysis. Nat Chem, 2012, 4: 349–354
2 Griffith L G, Naughton G. Tissue engineering-current challenges and expanding opportunities. Science, 2002, 295: 1009
3 Seyednejad H, Gawlitta D, Dhert W J A, et al. Preparation and characterization of a three-dimensional printed scaffold based on a functionalized polyester for bone tissue engineering applications. Acta Biomater, 2011, 7: 1999–2006
4 Therriault D, White S R, Lewis J A. Chaotic mixing in three-dimensional microvascular networks fabricated by direct-write assembly. Nat Mater, 2003, 2: 265–271
5 Lopes A J, MacDonald E, Wicker R B. Integrating stereolithography and direct print technologies for 3D structural electronics fabrication. Rapid Prototyping J, 2012, 18: 129–143
6 Gu D D, Meiners W, Wissenbach K, et al. Laser additive manufacturing of metallic components: Materials, processes and mechanisms. Int Mater Rev, 2012, 57: 133–164
7 Asgharzadeh H, Simchi A. Effect of sintering atmosphere and carbon content on the densification and microstructure of laser-sintered M2 high-speed steel powder. Mat Sci Eng A-Struct, 2005, 403: 290–298
8 Santos E C, Shiomi M, Osakada K, et al. Rapid manufacturing of metal components by laser forming. Int J Mach Tool Manu, 2006, 46: 1459–1468
9 Zheng Y, He Z, Gao Y, et al. Direct desktop printed-circuits-on-paper flexible electronics. Sci Rep, 2013, 3: 1786
10 Ladd C, So J H, Muth J, et al. 3D printing of free standing liquid metal microstructures. Adv Mater, 2013, 25: 5081–5085
11 Tabatabai A, Fassler A, Usiak C, et al. Liquid-phase gallium-indium alloy electronics with microcontact printing. Langmuir, 2013, 29: 6194–6200
12 Boley J W, White E L, Chiu G T C, et al. Direct writing of gallium-indium alloy for stretchable electronics. Adv Funct Mater, 2014
13 Kim G, Son J, Park S, et al. Hybrid process for fabricating 3D hierarchical scaffolds combining rapid prototyping and electrospinning. Macromol Rapid Comm, 2008, 29: 1577–1581
14 Chang S C, Bharathan J, Yang Y, et al. Dual-color polymer light-emitting pixels processed by hybrid inkjet printing. Appl Phys Lett, 1998, 73: 2561–2563
15 Li L, Saedan M, Feng W, et al. Development of a multi-nozzle drop-on-demand system for multi-material dispensing. J Mater Process Technol, 2009, 209: 4444–4448
16 Xu T, Binder K W, Albanna M Z, et al. Hybrid printing of mechanically and biologically improved constructs for cartilage tissue engineering applications. Biofabrication, 2013, 5: 015001
17 Mannoor M S, Jiang Z, James T, et al. 3D printed bionic ears. Nano Lett, 2013, 13: 2634–2639
18 Cahill D G, Pohl R O. Lattice-vibrations and heat-transport in crystals and glasses. Ann Rev Phys Chem, 1988, 39: 93–121